RSC Advances

PAPER

View Article Online
View Journal | View Issue

Cite this: *RSC Adv.*, 2016, **6**, 50112

Hierarchically porous carbon black/graphene hybrid fibers for high performance flexible supercapacitors†

Wujun Ma, Shaohua Chen, Shengyuan Yang and Meifang Zhu*

Received 6th April 2016
Accepted 16th May 2016

DOI: 10.1039/c6ra08799j

www.rsc.org/advances

To meet the rapid development of lightweight, flexible, and even wearable electronics, it is critically important to develop matchable, highly efficient energy-storage devices for their energy supply. Graphene fiber-based supercapacitors (SCs) are considered as one of the promising candidates because of the superior mechanical and electrical properties of graphene fibers. However, SCs based on neat graphene fibers generally suffer a low capacitance and poor rate performance, which largely restrict their potentially wide applications. Here, we report a simple, low cost and scalable wet-spinning method to fabricate porous carbon black/reduced graphene oxide (CB/rGO) hybrid fibers. The hybrid fibers possess very high surface area (254.6 m^2 g^{-1}) and a hierarchically porous nanostructure. A flexible solid-state SC was assembled using the hybrid fiber, which exhibited high capacitance (97.5 F cm^{-3}), excellent cycling stability (95.9% capacitance retention over 2000 cycles), superior energy density (2.8 mW h cm^{-3}) and ultrahigh power density (1200 mW cm^{-3}). Its physical shape and electrochemical performance is also very well maintained under long-time periodic mechanical deformation that is particularly promising for wearable electronic devices.

1. Introduction

Due to the fast development of portable and wearable electronics in our society, it is critically important to develop matchable flexible and highly efficient energy storage devices.[1–8] Supercapacitors (SCs), which are superior in ultrahigh power density, exceptional cycle life, and fast charging/discharging capacity, are widely recognized as important candidates for wearable electronics.[9–12] In our daily lives, fiber is one of the most common flexible materials. If the SCs are made in a wire or fiber format, they can satisfy the development of flexible and wearable electronics. Graphene fiber formed by individual graphene nanosheets is one of the promising candidates for flexible electrodes, because they are light, highly conductive, bendable, and even can be woven into wearable cloths. Up to now, many methods have been developed to fabricate graphene fibers.[13–26] However, due to the strong π–π stacking interaction between individual graphene sheets, aggregation or restacking inevitably occurs in the fibers,[27] which largely limits their application in supercapacitors that specifically require large surface areas and a porous structure.[28,29] To minimize the restacking, considerable efforts have been devoted to fabricate porous graphene fibers. Inserting nano spacers such as SWCNTs[30,31] and MoS_2 [32] into graphene sheets to expand their layer distance is an effective strategy to fabricate porous graphene hybrid fibers. However, the relatively high cost of SWCNTs and MoS_2 and non-continuous fabrication process for graphene fibers limit their practical application in flexible SCs. Consequently, it is still a great challenge to develop a scalable method to fabricate low cost porous graphene fibers for high performance flexible SCs.

Herein, low cost porous CB/rGO hybrid fibers were fabricated by a very simple, scalable wet-spinning method. Flexible solid-state SCs were assembled using these hybrid fibers and exhibited high capacitance of 97.5 F cm^{-3}, excellent cycling stability, superior energy density of 2.8 mW h cm^{-3} and ultrahigh power density up to 1200 mW cm^{-3}. Meanwhile, it maintained excellent physical and capacitive stability under bending deformation, indicating a good flexibility for flexible and wearable applications.

2. Experimental

2.1 Preparation of the fibers

Graphite oxide was synthesized by a modified Hummers method.[33] To obtain the hybrid fibers, CB (VXC-72R) and GO were mixed at weight ratios of 0 : 100, 10 : 90, 20 : 80 and 40 : 60 into distilled water. The mixtures (10 mg ml^{-1}) were sonicated for 2 h and then concentrated to 40 mg ml^{-1} by evaporation in 60 °C water bath. Continuous wet-spinning was carried out on

State Key Laboratory for Modification of Chemical Fibers and Polymer Materials, College of Material Science and Engineering, Donghua University, Shanghai 201620, P. R. China. E-mail: zhumf@dhu.edu.cn

† Electronic supplementary information (ESI) available. See DOI: 10.1039/c6ra08799j

a homemade apparatus.[26] Firstly, homogeneous dispersions were loaded into plastic syringes then injected into a rotating coagulation bath, the resulted gel fibers were rolled onto a drum and dried at 60 °C in vacuum. All GO and CB/GO fibers were reduced in an aqueous HI solution (45%, Sinopharm) at 95 °C for 12 h,[34] followed by ethanol washing and drying at 60 °C for 12 h in vacuum. The CB/rGO fibers with 10%, 20%, 40% CB loading contents are respectively named as CB/rGO Fiber-10, CB/rGO Fiber-20, and CB/rGO Fiber-40 hybrid fibers.

2.2 Material characterization

The morphology and microstructure of the fiber were measured by FE-SEM (HITACHI S4800). Tensile tests were carried on a XQ-1A fiber tension tester (Shanghai New Fiber Instrument) (extension rate of 2 mm min^{-1} with a gauge length of 10 mm). The resistivity was measured using a two probe method on a PC68 high resistance meter (Shanghai Cany Precision Instrument). Nitrogen adsorption–desorption isotherms of the fibers were measured at 77 K using Micromeritics ASAP2020.

2.3 Fabrication of the fiber-based SCs

Polyvinyl alcohol (3.0 g) was added to 27.0 g deionized water, followed by heating at 95 °C under magnetic stirring for 3 h. H_3PO_4 (3.0 g) was finally dropped to the above solution to form the gel electrolyte. To fabricate a fiber-based SCs, two fibers with the same diameter and length (1 cm) were connected to a metal wire by Ag paste, respectively, immersed in the H_3PO_4–PVA gel solution for 24 h, dried at room temperature until the gel electrolyte solidified, and placed on a Scotch tape in parallel. Finally another piece of tape was pasted on it to form a solid-state SCs.

2.4 Electrochemical characterization

The electrochemical performances of the assembled SCs were carried out using a two-electrode configuration on an electrochemical workstation (CHI 660E). The capacitance was calculated from CV curves using the equation

$$C = \frac{1}{2\Delta U v}\int |i(U)|\mathrm{d}U \quad (1)$$

where C is the total capacitance, v is the scan rate and ΔU is the potential window, $i(U)$ is the current.

C can be also calculated from GCD curves using

$$C = \frac{I\Delta t}{\Delta U} \quad (2)$$

where I and Δt are the discharging current and time, respectively.

The volumetric and mass capacitances (C_V and C_M) of the SC were calculated using the equations

$$C_V = \frac{4C}{V} \quad (3)$$

$$C_M = \frac{4C}{M} \quad (4)$$

where V and M refer to the volume and mass of the SC, respectively.

V is calculated according to the equation

$$V = 2\pi R^2 L \quad (5)$$

where R is the radius of the fiber, L is the fiber length, factor 2 means two fibers.

The volumetric energy (E_V) and power (P_V) density of the SCs were calculated using the equation

$$E_V = \frac{1}{8}C_V\Delta U^2 \quad (6)$$

$$P_V = E_V/\Delta t \quad (7)$$

3. Results and discussions

The porous CB/rGO fibers were continuously prepared through a simple scalable wet spinning method, followed by chemical reduction, as shown in Fig. 1. Firstly, CB and GO were mixed to form homogeneous spinning dopes, in which GO could act as a surfactant to disperse CB. Then the dope was smoothly injected into a rotating coagulation bath through a spinneret to obtain CB/GO fiber. The spinning velocity of CB/GO fibers is about 2 m min^{-1}, which can be further improved by adjusting the spinning conditions. Finally, the obtained CB/GO fibers were reduced by HI solution to form CB/rGO fibers. By this method, hundreds of meters long CB/rGO fibers can be obtained. To obtain the optimum composition, several fibers with different CB contents were fabricated. However, when the CB content is over 40%, the formed gel fiber is too weak to be collected.

The morphology and microstructure of the neat and hybrid fibers were measured by SEM in Fig. 2. It is obvious that for the neat rGO fiber without CB, the rGO sheets are packed very tightly due to the π–π interactions (Fig. 2a–c). While for CB/rGO hybrid fiber, the rGO sheets were effectively separated apart by CB, forming a hierarchically porous structure (Fig. 2d–f). Such an interconnected porous structure could largely increase the accessible surface areas and facilitate the electrolyte ions diffusion between rGO sheets when used as supercapacitor electrode.

The mechanical and electrical properties of the hybrid fibers were investigated, and results are shown in Fig. 3. Due to the presence of plenty of pores, the tensile strength decreases from

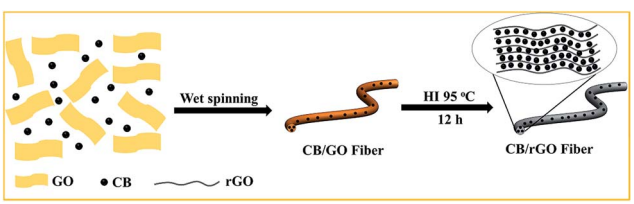

Fig. 1 Schematic of the fabrication of CB/rGO hybrid fibers.

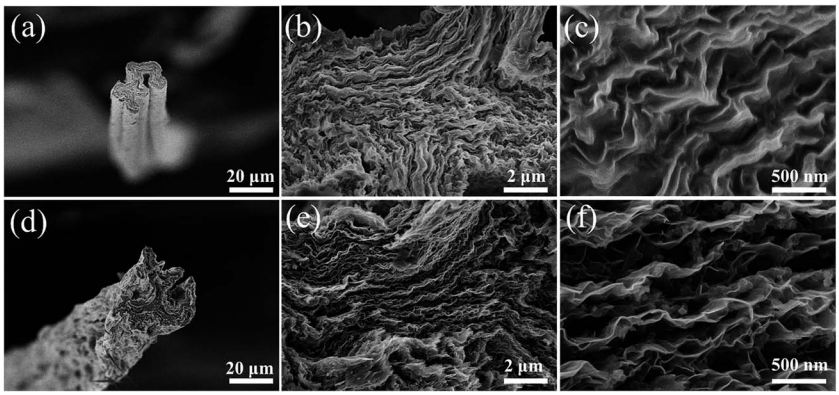

Fig. 2 SEM images of the cross-section of neat rGO fiber (a–c) and CB/rGO-40 hybrid fiber (d–f).

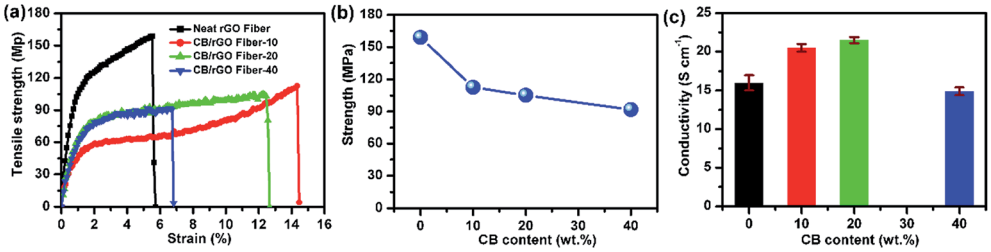

Fig. 3 Mechanical and electrical properties of the rGO and CB/rGO fibers. (a) Typical tensile stress–strain curves. (b) Dependence of the strength on the CB content. (c) Dependence of the electrical conductivity on the CB content.

159 MPa for the neat fiber to 92 MPa when the loading content of CB increases to 40%. However, the elongation at break is increased, indicating superior ductility for promising applications in flexible and wearable devices. The strength of CB/rGO-40 hybrid fiber is comparable with that of SWCNT/rGO fiber (84 MPa)[30] and rGO@CMC fiber (73 MPa).[31] When the CB content is increased, the electrical conductivity is surprisingly improved from 16 S cm^{-1} for the neat rGO fiber to 21.5 S cm^{-1} for CB/rGO Fiber-20, and then decreases slightly to 14.9 S cm^{-1}. A possible reason is that conductive CB nanoparticles provide plenty of conductive bridges between rGO sheets. But too many pores are created at a high CB content and would lead to decreased conductivity.

The specific surface area and microstructures of the obtained fibers were measured using nitrogen adsorption–desorption technique (Fig. 4a). The isotherm curve of CB/rGO-40 fiber shows type IV with a hysteresis loop,[35] suggesting the presence of mesopores in the CB/rGO fiber,[36] which is constructed by the stacked graphene sheets and CB.[37] The Brunauer–Emmett–Teller (BET) surface area of the CB/rGO-40 fiber was as high as 254.6 $m^2 g^{-1}$. By comparison, the neat rGO fiber showed a lower specific surface area of 13.4 $m^2 g^{-1}$, indicating

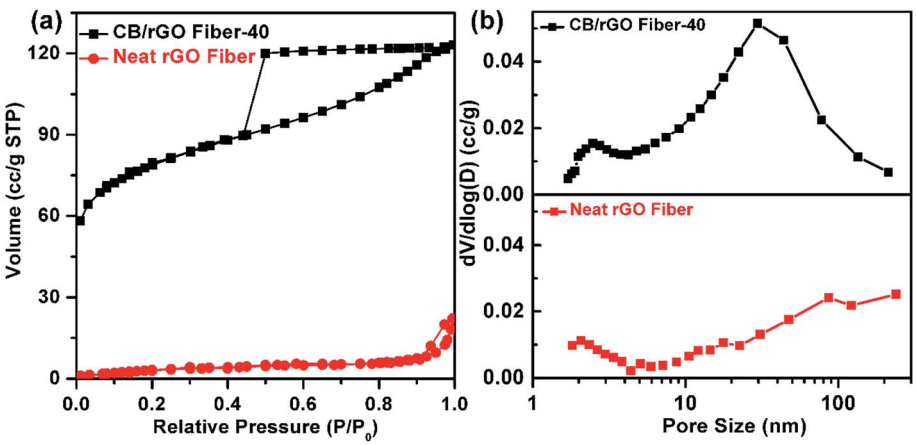

Fig. 4 (a) Nitrogen adsorption–desorption isotherms and (b) pore size distribution of the neat rGO fiber and CB/rGO-40 hybrid fiber.

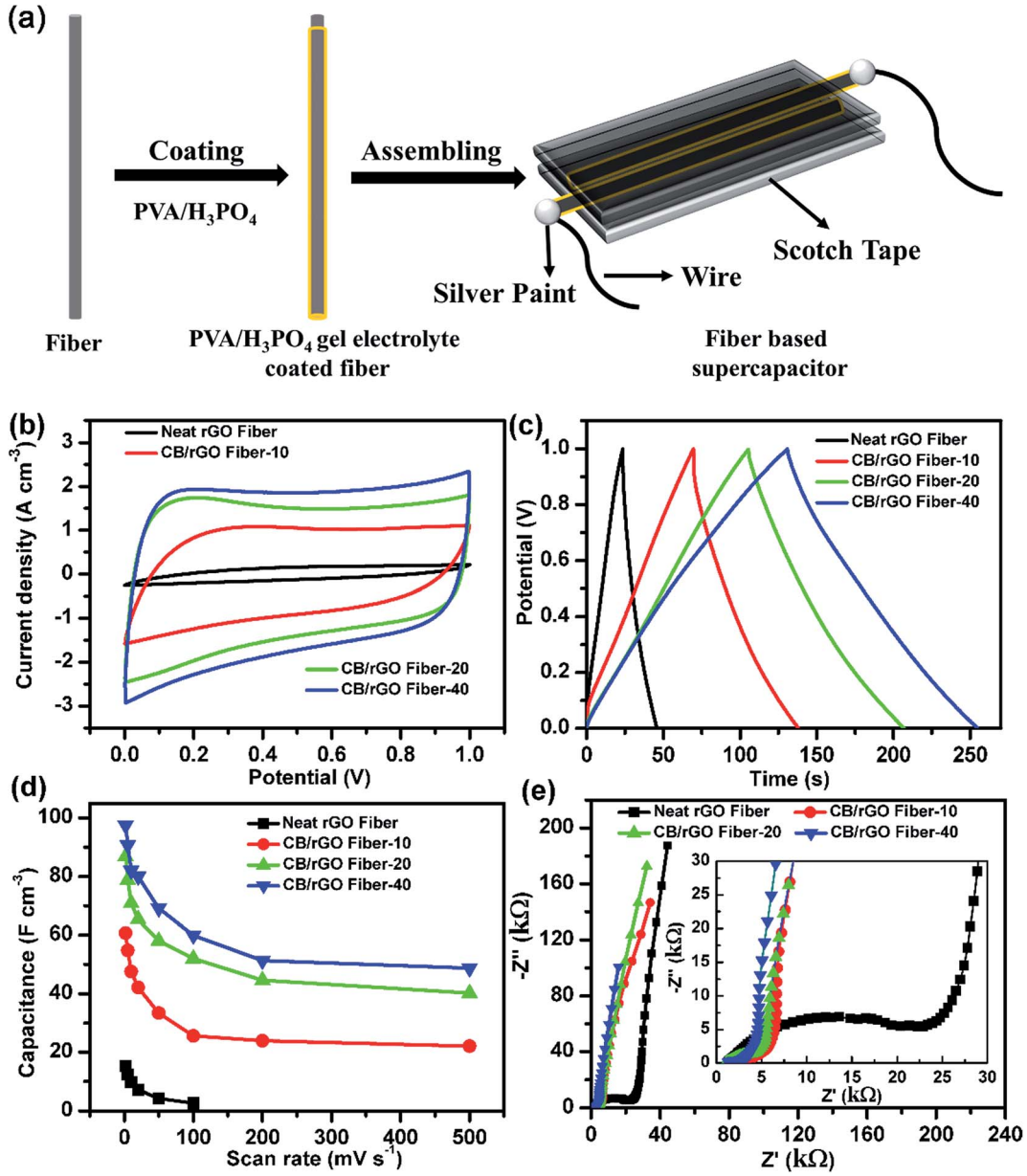

Fig. 5 (a) Scheme of the fabrication process of flexible solid-state supercapacitors based on the fibers. (b–e) Electrochemical performance of the SCs assembled from the neat rGO fibers and CB/rGO hybrid fibers. (b) CV curves at a scan rate of 50 mV s^{-1}. (c) GCD curves at a current density of 0.64 A cm^{-3}. (d) Volumetric capacitance of the SCs at different scan rates. (e) Nyquist plots of the SCs.

that the introduction of CB nanoparticles can efficiently prevent the agglomeration of the rGO sheets and form porous structure. The pore size distribution is shown in Fig. 4b. Clearly, almost no obvious peaks of mesopores existed in the neat rGO fiber (Fig. 4b), which is consistent with the low BET surface area, suggesting the serious restacking of the rGO sheets during drying. The CB/rGO-40 fiber shows a broad pore size distribution of 2–200 nm and two obvious peaks centered at 2.5 and 30 nm, suggesting the presence of mesopores and large pores in the fiber, which is consistent with the SEM images. Such hierarchical structure with high specific surface area and large fraction of mesopores could provide more favorable pathways for electrolyte penetration and more inner area for ion adsorption, thus facilitate the rapid charge–discharge and enhance the capacitance of the fiber electrode.[36]

To explore the electrochemical performance of the porous fibers, all solid-state wire-shaped SCs were fabricated according to the schematic in Fig. 5a. The PVA/H_3PO_4 gel was used as the electrolyte, and the Scotch tape worked as the substrate and the protection shield (Fig. 5a). The capacitive performances of the SCs based on the neat rGO and CB/rGO fibers were analyzed by using CV and GCD characterizations. As shown in Fig. 5b, the maximum current density and integrated area of the CV curves increases definitely with the loading content of CB at the same scan rate. Fig. 5c shows that all GCD curves are nearly symmetric, demonstrating a typical behavior of double layer

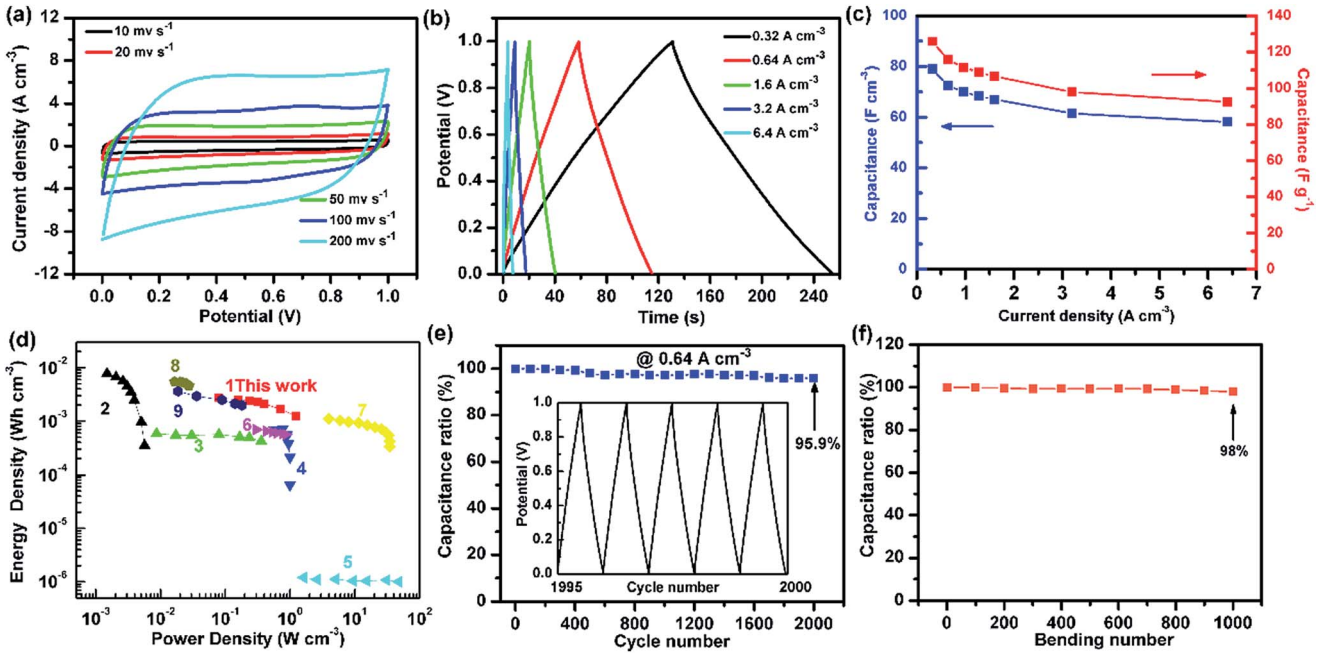

Fig. 6 Electrochemical performances of the CB/rGO-40 fiber based SC. (a) CV and (b) GCD curves of the SC. (c) Dependence of the volume- and mass-specific capacitance on current densities. (d) Ragone plots comparing our SC with commercial energy storage systems ((2) 4 V/500 μA h thin-film lithium battery, (3) 2.75 V/44 mF commercial SC, (4) 5.5 V/100 mF commercial AC-SC, (5) 3 V/300 μF Al electrolytic capacitor) and other fiber-shaped SCs ((6) MnO_2/carbon fiber, (7) PEDOT/CNT fiber/Pt wire, (8) MoS_2/RGO, (9) CNT/RGO@CMC fiber). (e) Dependence of capacitance ratio on the GCD cycle number. Inset: GCD curve after 2000 cycles at 0.64 A cm^{-3}. (f) Capacitance retention during 1000 bending cycles between a bending angle of 0° and 180°.

SCs. And the charge–discharge time obviously increases with the increasing CB content. The volumetric capacitances clearly increased with the increasing CB weight percentage (Fig. 5d) and the CB/rGO-40 fiber shows the highest capacitance of 97.5 F cm^{-3} at 2 mV s^{-1}, that is appropriately 7 times of the neat rGO fibers (15.3 F cm^{-3}) under the same condition. Furthermore, when the scan rate increases from 2 mV s^{-1} to 500 mV s^{-1}, the capacitance decreases to 48.7 F cm^{-3} corresponding to a retention rate of 50%, which indicates an excellent rate capability. This could be attributed to its small internal resistance (Fig. 5e).

The SC based on CB/rGO-40 hybrid fibers was carefully investigated. The CV curves in Fig. 6a show rectangular shapes even at a high scan rate of 200 mV s^{-1}, inferring their excellent rate performance. The charge–discharge behavior of the SC was also examined in the voltage range between 0 and 1 V (Fig. 6b). All the GCD curves maintained a typical triangular shape even at a high current densities up to 6.4 A cm^{-3}, indicating a nearly ideal capacitive behavior. The specific capacitance of the CB/rGO-40 fiber electrode is 79 F cm^{-3} (125.8 F g^{-1}) at a current density of 0.32 A cm^{-3} (Fig. 6c), which is substantially higher than those of a LC-spun RGO fiber (3.77 F cm^{-3} at 0.1 mA cm^{-2}),[38] a RGO core–sheath fiber (~38 F g^{-1} at 0.2 A g^{-1}),[19] and comparable to a polyaniline deposited RGO fiber (76.1 F cm^{-3} at 0.1 mA cm^{-2}).[38] As the current density increased to 6.4 A cm^{-3}, the CB/rGO-40 fiber electrode still showed a capacitance as high as 58.1 F cm^{-3} or 92.5 F g^{-1} (73.5% retention, Fig. 6c), implying an outstanding rate performance. This could be attributed to the hierarchically interconnected porous structure of the hybrid fiber (Fig. 2h), which could facilitate the rapid transport and migration of electrolyte ions during the charge/discharge process.

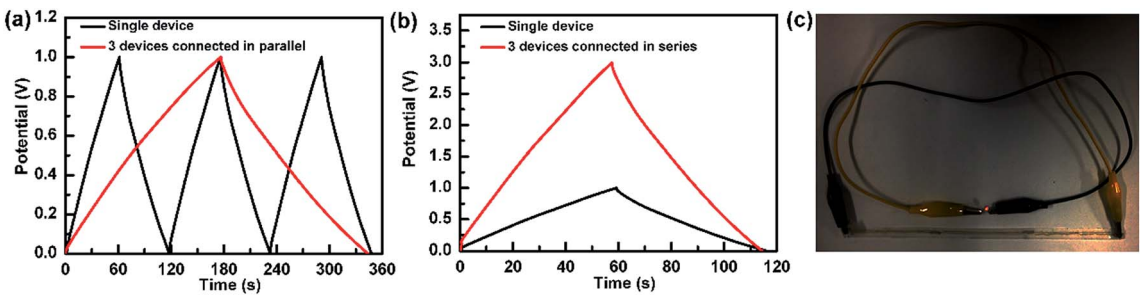

Fig. 7 GCD curves of single and three SCs connected in parallel (a) and series (b). (c) Photograph showing three as prepared SCs connected in series driving a red LED (1.8 V, 20 mA).

The Ragone plots in Fig. 6d show that the maximum energy density of our SC is up to 2.8 mW h cm^{-3} at the power density of 80 mW cm^{-3}, which is superior to those of commercially available SCs.[39,40] Compared with a Li-thin film battery, the SC exhibits significantly higher power densities while holds comparable energy densities.[41] This value is also higher than MnO_2@CNT fiber SC (1.73 mW h cm^{-3})[42] and the MnO_2-deposited carbon fiber SC (0.22 mW h cm^{-3}).[43] The volumetric power density can be up to 1200 mW cm^{-3}, which is superior to the CNT/RGO@CMC fiber SC (200 mW cm^{-3}),[31] the MoS_2/RGO fiber SC (200 mW cm^{-3})[32] and a CNT/RGO fiber SC (1080 mW cm^{-3}).[30] To now, the volumetric power density of our SC may be the highest among the graphene fiber-based SCs. The cyclic stability of the SC was explored by a galvanostatic charge/discharge test. The capacitance remained at 95.9% of the initial capacitance after 2000 cycles (Fig. 6e), the capacitance loss may be ascribed to the gradual degradation of redox groups in rGO, which was also reported for rGO fibers, CNT/rGO fibers and rGO films.[44–48] Furthermore, this SC is high flexibility and electrochemical stability under repeated bending cycles. As shown in Fig. 6f, it shows only 2% decay in capacitance after 1000 bending cycles between a bending angle of 0° and 180°.

To demonstrate the practical applications, we have connected three SCs together in series and/or parallel. The device was evaluated by GCD measurements. Fig. 7a shows that the discharge time of the three SCs connected in parallel is three times that of a single SC when operated at the same current density. With similar discharge time, the voltage window can be expanded from 1 V to 3 V by connecting three SCs in series (Fig. 7b), after charging at 3 V, it can efficiently power a red light-emission diode (LED) (Fig. 7c), demonstrating its potential application as an efficient energy storage component for flexible electronics.

4. Conclusion

In summary, a very simple and scalable wet-spinning method was developed to fabricate porous CB/rGO hybrid fibers with low cost. By introducing CB as spacers, the restacking of rGO sheets was effectively hindered. The hybrid fibers possess very high surface area and a hierarchically porous nanostructure. A flexible solid-state SC assembled from the CB/rGO-40 hybrid fibers exhibited high single-electrode capacitance, excellent cycling stability, and high energy density and outstanding power density. It also well maintained its physical shape and electrochemical performance under long-time periodical mechanical deformation. Besides, this work opens a door for the large-scale production of low cost hybrid graphene fibers with desirable high surface and hierarchical porous nanostructure for many critical applications such as water treatment and electrochemical sensors.

Acknowledgements

We acknowledge the financial supports from Natural Science Foundation of China (51273040) and National Natural Science Foundation for Distinguished Young Scholar of China (50925312).

References

1 H. Nishide and K. Oyaizu, *Science*, 2008, **319**, 737–738.
2 F. Lufrano, P. Staiti and M. Minutoli, *J. Power Sources*, 2003, **124**, 314–320.
3 Q. Cao, H.-s. Kim, N. Pimparkar, J. P. Kulkarni, C. Wang, M. Shim, K. Roy, M. A. Alam and J. A. Rogers, *Nature*, 2008, **454**, 495–500.
4 S. Ju, A. Facchetti, Y. Xuan, J. Liu, F. Ishikawa, P. Ye, C. Zhou, T. J. Marks and D. B. Janes, *Nat. Nanotechnol.*, 2007, **2**, 378–384.
5 J. F. Ihlefeld, P. G. Clem, B. L. Doyle, P. G. Kotula, K. R. Fenton and C. A. Apblett, *Adv. Mater.*, 2011, **23**, 5663–5667.
6 X. Zhang, L. Gong, K. Liu, Y. Cao, X. Xiao, W. Sun, X. Hu, Y. Gao, J. Chen, J. Zhou and Z. L. Wang, *Adv. Mater.*, 2010, **22**, 5292–5296.
7 X. Xiao, L. Yuan, J. Zhong, T. Ding, Y. Liu, Z. Cai, Y. Rong, H. Han, J. Zhou and Z. L. Wang, *Adv. Mater.*, 2011, **23**, 5440–5444.
8 Z. Yang, L. Li, Y. Luo, R. He, L. Qiu, H. Lin and H. Peng, *J. Mater. Chem. A*, 2013, **1**, 954–958.
9 P. Simon and Y. Gogotsi, *Nat. Mater.*, 2008, **7**, 845–854.
10 P. J. Hall, M. Mirzaeian, S. I. Fletcher, F. B. Sillars, A. J. R. Rennie, G. O. Shitta-Bey, G. Wilson, A. Cruden and R. Carter, *Energy Environ. Sci.*, 2010, **3**, 1238–1251.
11 C. Meng, C. Liu, L. Chen, C. Hu and S. Fan, *Nano Lett.*, 2010, **10**, 4025–4031.
12 G. Wang, L. Zhang and J. Zhang, *Chem. Soc. Rev.*, 2012, **41**, 797–828.
13 X. M. Li, T. S. Zhao, K. L. Wang, Y. Yang, J. Q. Wei, F. Y. Kang, D. H. Wu and H. W. Zhu, *Langmuir*, 2011, **27**, 12164–12171.
14 Z. Xu and C. Gao, *Nat. Commun.*, 2011, **2**, 571.
15 H. P. Cong, X. C. Ren, P. Wang and S. H. Yu, *Sci. Rep.*, 2012, **2**, 613.
16 Z. L. Dong, C. C. Jiang, H. H. Cheng, Y. Zhao, G. Q. Shi, L. Jiang and L. T. Qu, *Adv. Mater.*, 2012, **24**, 1856–1861.
17 E. Y. Jang, J. Carretero-González, A. Choi, W. J. Kim, M. E. Kozlov, T. Kim, T. J. Kang, S. J. Baek, D. W. Kim, Y. W. Park, R. H. Baughman and Y. H. Kim, *Nanotechnology*, 2012, **23**, 235601.
18 Z. Xu, Y. Zhang, P. G. Li and C. Gao, *ACS Nano*, 2012, **6**, 7103–7113.
19 Y. N. Meng, Y. Zhao, C. G. Hu, H. H. Cheng, Y. Hu, Z. P. Zhang, G. Q. Shi and L. T. Qu, *Adv. Mater.*, 2013, **25**, 2326–2331.
20 C. Xiang, C. C. Young, X. Wang, Z. Yan, C.-C. Hwang, G. Cerioti, J. Lin, J. Kono, M. Pasquali and J. M. Tour, *Adv. Mater.*, 2013, **25**, 4592–4597.
21 C. S. Xiang, N. Behabtu, Y. D. Liu, H. G. Chae, C. C. Young, B. Genorio, D. E. Tsentalovich, C. G. Zhang, D. V. Kosynkin, J. R. Lomeda, C. C. Hwang, S. Kumar, M. Pasquali and J. M. Tour, *ACS Nano*, 2013, **7**, 1628–1637.
22 Y. Zhao, C. C. Jiang, C. G. Hu, Z. L. Dong, J. L. Xue, Y. N. Meng, N. Zheng, P. W. Chen and L. T. Qu, *ACS Nano*, 2013, **7**, 2406–2412.

23 R. Jalili, S. H. Aboutalebi, D. Esrafilzadeh, R. L. Shepherd, J. Chen, S. Aminorroaya-Yamini, K. Konstantinov, A. I. Minett, J. M. Razal and G. G. Wallace, *Adv. Funct. Mater.*, 2013, **23**, 5345–5354.
24 J. Sun, Y. Li, Q. Peng, S. Hou, D. Zou, Y. Shang, Y. Li, P. Li, Q. Du, Z. Wang, Y. Xia, L. Xia, X. Li and A. Cao, *ACS Nano*, 2013, **7**, 10225–10232.
25 V. Chabot, D. Higgins, A. Yu, X. Xiao, Z. Chen and J. Zhang, *Energy Environ. Sci.*, 2014, **7**, 1564–1596.
26 S. Chen, W. Ma, Y. Cheng, Z. Weng, B. Sun, L. Wang, W. Chen, F. Li, M. Zhu and H.-M. Cheng, *Nano Energy*, 2015, **15**, 642–653.
27 X. Yang, J. Zhu, L. Qiu and D. Li, *Adv. Mater.*, 2011, **23**, 2833–2838.
28 Z. Fan, J. Yan, L. Zhi, Q. Zhang, T. Wei, J. Feng, M. Zhang, W. Qian and F. Wei, *Adv. Mater.*, 2010, **22**, 3723–3728.
29 N. Jung, S. Kwon, D. Lee, D.-M. Yoon, Y. M. Park, A. Benayad, J.-Y. Choi and J. S. Park, *Adv. Mater.*, 2013, **25**, 6854–6858.
30 D. Yu, K. Goh, H. Wang, L. Wei, W. Jiang, Q. Zhang, L. Dai and Y. Chen, *Nat. Nanotechnol.*, 2014, **9**, 555–562.
31 L. Kou, T. Huang, B. Zheng, Y. Han, X. Zhao, K. Gopalsamy, H. Sun and C. Gao, *Nat. Commun.*, 2014, **5**, 3754.
32 G. Sun, J. Liu, X. Zhang, X. Wang, H. Li, Y. Yu, W. Huang, H. Zhang and P. Chen, *Angew. Chem.*, 2014, **126**, 12784–12788.
33 W. S. Hummers and R. E. Offeman, *J. Am. Chem. Soc.*, 1958, **80**, 1339.
34 S. Pei, J. Zhao, J. Du, W. Ren and H.-M. Cheng, *Carbon*, 2010, **48**, 4466–4474.
35 J. Hu, Z. Kang, F. Li and X. Huang, *Carbon*, 2014, **67**, 221–229.
36 A. Bello, F. Barzegar, D. Momodu, J. Dangbegnon, F. Taghizadeh, M. Fabiane and N. Manyala, *J. Power Sources*, 2015, **273**, 305–311.
37 H.-F. Ju, W.-L. Song and L.-Z. Fan, *J. Mater. Chem. A*, 2014, **2**, 10895–10903.
38 T. Huang, B. Zheng, L. Kou, K. Gopalsamy, Z. Xu, C. Gao, Y. Meng and Z. Wei, *RSC Adv.*, 2013, **3**, 23957–23962.
39 M. F. El-Kady and R. B. Kaner, *Nat. Commun.*, 2013, **4**, 1475.
40 M. F. El-Kady, V. Strong, S. Dubin and R. B. Kaner, *Science*, 2012, **335**, 1326–1330.
41 D. Pech, M. Brunet, H. Durou, P. Huang, V. Mochalin, Y. Gogotsi, P.-L. Taberna and P. Simon, *Nat. Nanotechnol.*, 2010, **5**, 651–654.
42 J. Ren, L. Li, C. Chen, X. L. Chen, Z. B. Cai, L. B. Qiu, Y. G. Wang, X. R. Zhu and H. S. Peng, *Adv. Mater.*, 2013, **25**, 1155–1159.
43 X. Xiao, T. Li, P. Yang, Y. Gao, H. Jin, W. Ni, W. Zhan, X. Zhang, Y. Cao, J. Zhong, L. Gong, W.-C. Yen, W. Mai, J. Chen, K. Huo, Y.-L. Chueh, Z. L. Wang and J. Zhou, *ACS Nano*, 2012, **6**, 9200–9206.
44 X. Zhao, Q. Zhang, D. Chen and P. Lu, *Macromolecules*, 2010, **43**, 2357–2363.
45 Y. Ma, P. Li, J. Sedloff, X. Zhang, H. Zhang and J. Liu, *ACS Nano*, 2015, **9**, 1352–1359.
46 R. Ramachandran, M. Saranya, V. Velmurugan, B. Raghupathy, S. Jeong and A. Grace, *Appl. Energy*, 2015, **153**, 22–31.
47 Y. Zhao, Z. Zhang, Y. Ren, W. Ran, X. Chen, J. S. Wu and F. Gao, *J. Power Sources*, 2015, **286**, 1–9.
48 Y. Zhao, W. Ran, J. He, Y. Huang, Z. Liu, W. Liu, Y. Tang, L. Zhang, D. Gao and F. Gao, *Small*, 2015, **11**, 1310–1319.